

The Convective Storm Initiation Project

Keith A. Browning, 1 Alan M. Blyth, 2 Peter A. Clark, 3 Ulrich Corsmeier, 4
Cyril J. Morcrette, 1 Judith L. Agnew, 5 Sue P. Ballard, 3 Dave Bamber, 6
Christian Barthlott, 4 Lindsay J. Bennett, 2 Karl M. Beswick, 7 Mark Bitter, 8
Karen E. Bozier, 9 Barbara J. Brooks, 2 Chris G. Collier, 9
Fay Davies, 9 Bernhard Deny, 4 Mark A. Dixon, 3 Thomas Feuerle, 8
Richard M. Forbes, 3 Catherine Gaffard, 10 Malcolm D. Gray, 7 Rolf Hankers, 8
Tim J. Hewison, 10 Norbert Kalthoff, 4 Samiro Khodayar, 4 Martin Kohler, 4
Christoph Kottmeier, 4 Stephan Kraut, 4 Michael Kunz, 4 Darcy N. Ladd, 11
Humphrey W. Lean, 3 Jürgen Lenfant, 4 Zhihong Li, 3 John Marsham, 2
James McGregor, 6 Stephen D. Mobbs, 2 John Nicol, 1 Emily Norton, 7
Douglas J. Parker, 2 Felicity Perry, 2 Markus Ramatschi, 12 Hugo M. A. Ricketts,
7 Nigel M. Roberts, 3 Andrew Russell, 7 Helmut Schulz, 8 Elizabeth C. Slack, 11
Geraint Vaughan, 7 Joe Waight, 11 Robert J. Watson, 13 Ann R. Webb, 7
David P. Wareing, 14 Andreas Wieser, 4

1. Department of Meteorology, University of Reading, Reading, UK
2. Institute for Atmospheric Science, School of Earth and Environment,
University of Leeds, Leeds, UK
3. Met Office Joint Centre for Mesoscale Meteorology, University of Reading, UK
4. Institut für Meteorologie und Klimaforschung, Forschungszentrum
Karlsruhe/Universität Karlsruhe, 76021 Karlsruhe, Germany
5. Radio Communications Research Unit, Space Science and Technology Department,
Rutherford Appleton Laboratory, Chilton, UK
6. Cardington Field Site, Met Office, Cardington Airfield, UK
7. School of Earth, Atmospheric, and Environmental Sciences, University of
Manchester, Manchester, UK
8. Institut für Flugführung Universität Braunschweig 38108 Braunschweig, Germany
9. School of Environment & Life Sciences, University of Salford, Salford, UK
10. Met Office, Exeter, UK
11. CCLRC Chilbolton Observatory, Chilbolton, UK
12. Department 1: Geodesy and Remote Sensing, GFZ - Potsdam, Potsdam, Germany

13. Dept. of Electronic and Electrical Engineering, University of Bath, Bath, UK

14. Dept Physics, University of Wales at Aberystwyth.

Corresponding author address: Alan M Blyth, Institute for Atmospheric Science,
School of Earth and Environment, University of Leeds, Leeds, LS2 9JT, UK. E-mail:
blyth@env.leeds.ac.uk

Abstract

The Convective Storm Initiation Project (CSIP) is an international project to understand precisely where, when and how convective clouds form and develop into showers in the mainly maritime environment of southern England. A major aim of CSIP is to compare the results of the very-high-resolution UK Met Office weather

forecasting model with detailed observations of the early stages of convective clouds and to use the newly gained understanding to improve the predictions of the model.

A large array of ground-based instruments plus two instrumented aircraft, from the (UK) National Centre for Atmospheric Science (NCAS) and the Institute for Meteorology and Climate Research (IMK) Karlsruhe, were deployed in southern England, over an area centered on the meteorological radars at Chilbolton, during the summers of 2004 and 2005. In addition to a variety of ground-based remote-sensing instruments, numerous radiosondes were released at one- to two-hourly intervals from 6 closely-spaced sites. The Met Office weather radar network and Meteosat satellite imagery were used to provide context for the observations made by the instruments deployed during CSIP.

This article presents an overview of the CSIP field campaign and examples from CSIP of the types of convective initiation phenomena that are typical in the UK. It shows the way in which certain kinds of observational data are able to reveal these phenomena, and gives an explanation of how the analyses of data from the field campaign will be used in the development of an improved very-high-resolution NWP model for operational use.

Capsule

A major international project to understand the processes responsible for the initiation of convective storms was held in the mainly maritime environment of southern England.

1 Introduction

Flooding caused by heavy rain is a problem that is motivating renewed research in several countries and it is a major focus for international activities such as the World Weather Research Program. One of the greatest uncertainties in generating warnings of possible flood situations is in the prediction of the local distribution and timing of the rain. Thunderstorms - and rain associated with deep convection in general - are an important ingredient in many high-impact events such as flash floods, but the present capability for forecasting convection is especially poor. Such events are highly localized and very-high-resolution (of the order of 1 km grid) numerical-weather-prediction models are needed to represent them. The triggering of deep

convection is well understood in broad terms (e.g., Bennett et al. 2006), but not yet in sufficient detail to know how best to represent it within the models. A key task facing the meteorological community is thus to gain a better understanding of why deep convection breaks out *precisely where and when* it does and then to use such understanding in the development of improved NWP models. These were the goals of a recent experiment in the UK known as the Convective Storm Initiation Project, or CSIP.

CSIP was one of three complementary field campaigns. One of these, known as IHOP_2002 (Weckwerth et al. 2004), during the summer of 2002 in the U.S. southern Great Plains, was in a region characterized by large convective instability and strong capping inversions. The local orographic variations in this region are small and generally not critical to the triggering of convection. Another campaign, known as the Convective and Orographically Induced Precipitation Study (COPS), planned for summer 2007, will be in southwestern Germany / eastern France; this region is also characterized by large convective instability but with a major orographic influence. The CSIP field campaigns during the summers of 2004 and 2005, on the other hand, were in a region of the UK characterized by an intermediate level of orography together with nearby coastlines. The mainly maritime nature of the British climate and the remoteness of any major mountainous areas means that the convective instability and capping inversions are often quite weak on convective occasions. Only one of the cases encountered during CSIP was due to convection originating from a layer above the boundary layer; all of the other cases were due to convection initiating in the boundary layer. Elevated convective initiation events were much commoner in the IHOP_2002 experiment where about half the events were of that kind (Wilson and Roberts 2006).

2 Science issues addressed by CSIP

A characteristic feature of the atmosphere in situations leading to the outbreak of deep convection is the stable-layer phenomenon we refer to in this article as a lid. A lid is a layer of warm, dry air that traps air of high wet-bulb potential temperature (θ_w), usually in the boundary layer, beneath potentially colder air in the middle and upper troposphere. The nature of lids is illustrated by the sounding in Fig. 1. Imagine a parcel of warm, moist air originating close to the surface with a $\theta_w = 14^\circ\text{C}$. If it were lifted moist adiabatically (along the thin curve in Fig. 1) it would be warmer than its environment at most levels up to 480 hPa; the dark-gray shaded area in Fig.1 is a measure of the Convective Available Potential Energy (CAPE). However, this sounding also shows a relatively dry, warm layer between 740 and 610 hPa (lightly shaded) where this is not so. If the parcel were lifted to these levels it would be negatively buoyant. Such layers give rise to so-called Convective INhibition (CIN) and they act as lids that tend to inhibit the onset of deep convection. The lid in Fig. 1 is higher than typically observed on thunderstorm days in the US Great Plains region where IHOP was conducted (e.g. Weckwerth et al. 2004).

A lid assists in the build-up of latent instability by allowing warm, moist air to be bottled-up at low levels, thereby increasing CAPE. However, to realise the potential for deep convection, it is necessary for the low-level air eventually to be able to penetrate the lid. One way to achieve this is through progressive warming and/or moistening of the low-level air, perhaps as part of a diurnal trend. Identifying precisely where the convection will initially break through is a major challenge for prediction. The site of the initial outbreak will be influenced partly by any spatial

variability in the temperature and/or humidity of the boundary-layer air, perhaps on scales too small to be resolved by conventional observations (e.g., Weckwerth 2000). Sometimes the variability is due to the effects of variable terrain height or differing land- (or sea-) surface characteristics, or perhaps differential shadowing by cloud at higher levels.

Variability in the characteristics of the boundary-layer air may not, however, be the sole or even the principal determinant of precisely where the first deep convection will break out. The other factor that is important in the UK is variability in the strength of the lid itself. This can be either intrinsic variability owing to the differing source regions for different parts of the lid, or local variability owing to some mesoscale dynamical mechanism that lifts the lid locally. Such lifting will cool the lid rapidly (at the dry adiabatic rate), thereby eliminating the CIN and enabling boundary-layer air of high θ_w (ascending moist adiabatically) to penetrate it.

Even a small vertical displacement of the lid may be sufficient to allow the underlying air to penetrate buoyantly upward. This is illustrated in Fig. 2 which depicts another low-CIN situation, common in a maritime climate such as the UK's, in which a mere 15 hPa of lift (i.e. about 150 m) is enough to initiate deep convection. Sometimes the existence or otherwise of an appropriate local lifting mechanism will determine whether deep convection will be triggered at all: it can make the difference between an entirely dry day and the occurrence of a severe rainstorm. On other occasions, when the diurnal warming of the boundary layer is sufficient on its own to initiate deep convection, although the distribution of θ_w within the boundary layer may determine *broadly* where the initial convection will occur, the local distribution in the lifting of a lid (or local variability in the strength of an unperturbed lid) will

often still be the key to determining *precisely where and when* the first convection breaks out. Predicting the location of the first outbreak accurately is crucial because, once the first convective storm has formed, secondary processes are likely to take over which tend to control further convective initiation in the vicinity of the storm.

It has long been recognized that local lifting often occurs in the form of boundary-layer convergence lines, detectable by satellite (Purdom 1982) and seen by radar as fine lines of enhanced reflectivity (Wilson and Schreiber 1986). Convergence lines were particularly common during IHOP_2002 and where they intersected with other convergence lines they were often preferred locations for enhanced ascent and convective initiation. Some convergence lines are due to topographical effects such as those produced by variations in terrain height or land/water boundaries. During the VERTIKATOR-project in south-western Germany in 2002 topographically induced convergence lines proved to trigger deep convection over the Black Forest mountains (Barthlott et al. 2006). Others are due to variations in land-use or land-wetness, with associated variations in Bowen ratio (see references in Weckwerth and Parsons 2006). Also, under conditions of strong low-level shear, horizontal convective rolls, i.e. parallel lines of convergence separated by regions of divergence, oriented roughly along the direction of the shear, are an intrinsic dynamical feature of mixed boundary layers.

Triggering of deep convection that any of the above kinds of convergence line produce is referred to as primary initiation. Once the first storm has developed, this can, as already mentioned, lead to secondary initiation. The secondary initiation may arise from lifting by gravity waves emanating from an earlier storm or from lifting along its rain-chilled outflow (gust front) as it advances like a density current.

According to Wilson and Roberts (2006), just over half the convective-storm complexes, probably most of the cases with surface-based convection, associated with initiation episodes in IHOP_2002 produced gust fronts. Most of the long-lived events were associated with gust fronts.

Lifting can also result from ascent induced beneath travelling positive anomalies in potential vorticity occurring at upper levels. These PV anomalies are associated with tropopause depressions or folds (Hoskins et al. 1985). Such PV anomalies are often encountered in Europe and presumably in other middle or high latitudes and their influence on precipitation has been examined, for example, during the Mesoscale Alpine Programme (MAP; Bougeault et al. 2001). They are especially important because, as well as reducing the CIN through the induced lifting, they also increase the CAPE owing to the pool of cold air at middle and upper levels that always accompanies them.

In the remainder of this article we shall (i) provide an overview of the CSIP field campaign, (ii) present examples from CSIP of the types of convective initiation phenomena that are typical in the UK, showing the way in which certain kinds of observational data are able to reveal these phenomena, and (iii) explain how the analyses of data from the field campaign will be used in the development of an improved very-high-resolution NWP model for operational use. A large database has been accumulated from CSIP. Analysis is still at an early stage and the material presented here is intended to provide an overview of important processes, and of opportunities for improving forecasting models, rather than to give definitive results.

3 The CSIP field campaign

The main field campaign was conducted over southern England during June, July and August 2005. It benefited from an earlier pilot campaign in the same region in July 2004. An overview of the observational set-up is given in Fig. 3. The Operations Centre was based at Chilbolton (at the centre of the range rings in Fig. 3). This is the site of the Chilbolton radar facility with its 25-m steerable dish (Goddard et al. 1994). Other instruments were sited within range of the Chilbolton radars as shown in Fig. 3. Many of them were new or upgraded systems operated as part of the recently established (UK) Universities Facility for Atmospheric Measurement (UFAM) by staff from the Universities of Aberystwyth, Leeds, Manchester, Reading and Salford. The others were state-of-the-art instruments from the Institute for Meteorology and Climate Research (IMK), Karlsruhe, Germany, the Rutherford Appleton Laboratory, the Met Office, GFZ - Potsdam, and the University of Bath.

The observations

The set of instruments deployed in southern England for CSIP included

- 1275 MHz (L-band), 3 GHz (S-band) and 35 GHz Doppler radars at Chilbolton (the 3 GHz radar is also a polarization radar)
- UHF wind profiler
- 3 Sodars
- 2 Doppler lidars
- Ozone lidar
- Water vapor lidar
- 3 microwave radiometers

- Ceilometer
- Serial ascents at 1 to 2 h intervals from 6 mobile rawinsonde stations, plus serial ascents from 3 UK Met Office operational systems (giving a total of about 800 soundings associated with CSIP)
- Network of 16 automatic weather stations
- 2 instrumented light aircraft (DO 128 and Cessna 182)
- Network of 5 GFZ GPS integrated water vapor stations
- 2 energy-balance stations

These instruments were within a region of good coverage by the Met Office network of surface stations and the UK operational weather radar network, which provided maps of estimated rainfall intensity at resolutions mainly between 1 and 2 km every 5 min for single radars and every 15 min for composite displays. Extensive use was made of infrared, water vapor and high-resolution visible imagery every 15 min from Meteosat 8, the Meteosat Second Generation (MSG) satellite (Schmetz et al. 2002) and every 10 min from Meteosat-6. These products were used not only for post-storm analysis, but also for nowcasting to guide deployment of aircraft and serial rawinsondes. Hourly surface-wind and convergence analyses from the Met Office NIMROD system (Golding 1998) were also used for this purpose.

Forecasting products

The most useful products for forecasting convection initiation were those derived from the operational mesoscale version of the Unified Model (Cullen 1993) which was run every 6 h out to T+36h on a 12-km grid. These runs were supplemented by special runs from a 4-km version of the Unified Model being

developed by Met Office staff at the Joint Centre for Mesoscale Meteorology (JCMM) at the University of Reading. An example of these products is shown in Fig. 4. Figures 4(a) and 4(b) depict the T+13h forecasts of rainfall intensity in the CSIP operating area on 29 June 2005, from the 12- and 4-km versions of the model, respectively. Figure 4(c) depicts the corresponding observed pattern of rainfall obtained by the weather radar network.

Both models use the new non-hydrostatic, fully compressible deep atmosphere dynamical core (Davies et al. 2005). The 12-km model uses a 3-hour, 3D-VAR data assimilation cycle (Lorenc et al. 2000) supplemented by assimilation of cloud and radar-based rainfall information using nudging techniques (Jones and Macpherson 1997). It provides a well-proven mesoscale background but uses a parameterization of deep convection based on Gregory and Rowntree (1990). Essentially it is an equilibrium mass-flux scheme, tending to respond to CAPE, and it gives only a general indication of areas where convection is possible, with little fine-scale detail. The 4-km model, run one-way nested within the 12-km model and using the same initial conditions, follows its mesoscale evolution closely but benefits in two ways. First, it resolves surface forcing and resulting flow much better, and so often provides better guidance as to the areas where surface-forced initiation is most likely. Second, while the mass-flux parameterization is still used, its mass-flux is limited in such a way as to ensure that deep convection is treated largely explicitly. Although a 4-km grid is not ideal, it has been shown to behave adequately when compared with 1-km versions of the same model in cases of intense convection. In particular, mechanisms leading to mesoscale organisation are captured quite well. The inadequate resolution does tend to lead to a delay in initiation of order an hour, but spatial guidance is often superior to that from the 12-km model.

Another useful product for forecasting convective initiation obtained from the operational run of the mesoscale model that we wish to highlight was a time-height plot of forecast θ_s , or saturation potential temperature, above the lifting condensation level. θ_s is the dry-bulb temperature read off on the θ_w scale as though the air were saturated. The plot has the advantage of showing at a glance the expected evolution of layers of CAPE and of CIN (i.e. lids) with respect to any parcel value of θ_w . An example is given in Fig. 5. The upper panel of Fig. 5 shows a lid with θ_s up to 17°C just above the lifting condensation level (white curve) at heights between 1 and 2 km from 1530 to 2100 UTC (on Day 1). Predicted surface values of θ_w , plotted along the bottom of the lower panel, were not quite high enough during this period for parcels to penetrate the unmodified lid, although the predicted maximum surface value of θ_w at 1600 UTC (16.7°C) would have produced parcels with a 1°C temperature excess at the 4-km level if they could have penetrated the lid. In the event, low-level convergence is believed to have lifted (and hence weakened) the lid locally and allowed convection to penetrate upward to 6 km at around 1700 UTC. Illustrations of this kind of behavior are shown below.

4 Observing the pre-storm lids and convective elements

CSIP is concerned specifically with *initiation* of convection and so it was important to be able to observe the detailed structure of the pre-storm boundary layer, of the lid (or lids) capping it, and of convective elements (clear-air thermals, fair-weather cumulus and cumulus congestus) before, during and just after they penetrated

the lid. Thermodynamic information on the structure of the boundary layer and lids is available in CSIP from the serial rawinsondes and aircraft traverses. This information is supplemented by data from the 3 GHz and 1275 MHz high-power radars at Chilbolton. As shown in the following example, these radars provided important information on the nature and detailed pattern of the pre-storm boundary layer, lids, and convection on scales of tens of kilometres down to hundreds of metres.

Two kinds of scattering mechanisms are involved in the detection of the above features by radar. Echoes from the edges of convective elements are generally due to Bragg scattering from refractive index inhomogeneities, mainly from humidity gradients (Doviak and Zrnic 1993). Echoes in the interiors of convective elements are more often due to Rayleigh scattering from large cloud particles, precipitation or perhaps insects. Layer echoes can be due to Bragg scatter or Rayleigh scatter from insects. The 3 GHz and 1275 MHz radars are mounted on the same dish and are operated at the same time. Having data simultaneously from the two radars is beneficial in that the different wavelength dependency of Bragg and Rayleigh scattering helps clarify the nature of the targets (scattering by refractive index inhomogeneities is favored at 1275 MHz compared to 3 GHz).

Figure 6 shows examples of RHI scans from the 3 GHz radar. Figure 6(a) depicts a layer of low-reflectivity echo from the bottom of a lid above a cloud-free boundary layer prior to the development of significant convection beneath it. Figure 6(b) depicts echoes not only from a lid some way above the boundary layer but also from the edges of clear-air thermals and fair-weather cumulus clouds as the top of the convective boundary layer began to rise up toward the lid.

Figure 7 shows another RHI scan from the 3 GHz radar but this time it shows differential reflectivity (ZDR)¹ rather than reflectivity (Z). It depicts in green the echoes from the edges of large cumulus congestus clouds as well as from the precipitation particles developing within them. However, unlike in all the other cases during CSIP, where the convection originated from the boundary layer, the convection here was occurring in the form of elevated convection from air being advected above a stable frontal zone that is depicted by multiple red/maroon echo layers. Here the lid that would previously have restrained the convection is no longer evident. The lid would have been situated at the top of the boundary-layer air before it was advected from France and lifted above the frontal zone.

The fact that Fig. 7 depicts ZDR rather than Z explains why the echoes from the convective cells are so easily distinguishable from the layer echoes within the stable frontal zone (i.e. green versus red/maroon). The green echoes have low values of ZDR typical of both Bragg scattering from refractive index inhomogeneities at the edges of the convective cells and of Rayleigh scattering from newly developing precipitation. The red/maroon echoes were probably due to elongated insects advected within the frontal zone.

Figure 8, an RHI scan from the 1275 MHz radar, shows an example of the radar signature of cumulus congestus clouds. It depicts the reflectivity from two such clouds, each 3 km high, that had only recently penetrated a lid capping the boundary layer at about 1 km (Morcrette et al. 2006). In the case of the cloud at 18 to 20 km range, the radar detects just the Bragg scatter from the refractive index

1 Differential reflectivity (ZDR) is the ratio between the horizontal and vertical received power and is thus a measure of the oblateness of the scatterers.

inhomogeneities at the cloud boundaries. In the case of the cloud at 10 to 13 km range it may be detecting also the Rayleigh scatter from precipitation particles developing within it; alternatively it may be seeing mainly Bragg scatter, but from the edges of a cluster of smaller sub-cells. The breakthrough of convective cells above the lid, as in Fig. 8, often occurs where the lid is lifted locally by some mesoscale mechanism; examples of these mechanisms are presented shortly.

We suspect that mesoscale lifting processes are the mechanism responsible for localizing the initiation of convection on the majority of occasions; however, convective break-through can in principle be localized even without local lifting provided the lid is weak and there are significant local hot spots or moist anomalies within the boundary layer. Thus before proceeding to look at the mesoscale lifting mechanisms, we shall present one more radar product used in CSIP – one that can reveal the mesoscale variability in the structure on a roughly horizontal plane within the boundary layer itself. Figure 9 shows the near-surface refractivity (N) field derived from the 1275 MHz radar using the technique pioneered by Fabry et al. (1997). The technique utilises the change in phase of radar returns from ground targets relative to a reference scan. The reference scan was chosen to correspond to a near-constant refractivity field as determined by observations from the 16 automated weather stations surrounding Chilbolton. During summer, day-time conditions, the refractivity field is primarily influenced by variations in humidity, where a change of 1 unit corresponds to a change in relative humidity of approximately 1%. Although limited mainly to ranges within 30 km of the radar at Chilbolton, the technique provides valuable insight into scales of variability not easily resolved by the *in situ* measurements. Figure 9 shows a large gradient in refractivity just to the north-west of the radar (at Chilbolton), corresponding to a relative humidity gradient of

approximately 10%. A corresponding gradient in moisture was detected by radiosondes released from Chilbolton and Larkhill, 25 km west of Chilbolton. Satellite pictures showed that convective clouds developed in the moist region.

5 Observing the mesoscale forcing mechanisms within the boundary layer

Localized lifting is usually the key to determining precisely where and when convection will be triggered. Our belief that local variability in boundary-layer moisture plays only a secondary role to mesoscale lifting processes in localizing convective initiation is in line with the analyses of IHOP_2002 data by Fabry (2006). A variety of types of mesoscale forcing were observed during the 18 Intensive Observing Periods (IOPs) of the main 2005 field campaign. Some examples are presented below from these IOPs and also from one of the cases observed during the 2004 pilot project. Three of these examples illustrate forcing from low levels and two illustrate forcing from upper levels.

Examples of boundary-layer forcing

We first present examples of primary initiation along convergence lines within the boundary layer. Figure 10 is a visible satellite image showing clouds along a convergence line that trailed persistently downwind from the south coast of south-west England. An RHI scan across this line (Fig. 11) illustrates the effects of the convergence. The reflectivity plot in Fig. 11(a) and the ZDR plot in Fig. 11(b) both show two clear-air layers as well as one of the shower clouds that formed along the convergence line (at 53 km). Most of the echo in the ZDR plot – both layer and convective echo – is probably due to Bragg scattering, i.e. low ZDR (green); however,

the low-ZDR echo at the top of the shower cloud may be due to ice particles above the 3-km 0 degC level and the higher-ZDR echo coinciding with the reflectivity core is due to rain (produced, at least in part, from melting ice rather than from the warm-rain process alone). The undulating echo ‘layer’ around 1 km, detectable from minimum range out to 50 km, is not so much a layer as an envelope of small convective elements in the boundary layer. Above this, there is another, somewhat smoother echo layer at about 2 km that rises to over 2.5 km beyond 40 km, reaching a peak where the main shower cloud is developing. This echo layer corresponds to the base of the major lid at 750 hPa seen in the sounding in Fig. 1. The small shower cloud and the locally raised lid are both manifestations of the convergence line.

A second example of primary initiation is given in Fig. 12 which shows convective cloud streets along boundary-layer convergence lines (horizontal convective rolls) almost parallel to the strong low-level wind. The clouds (Fig. 12(a)) formed as the airflow progressed inland into southern England. They started to develop in the early morning and by midday they were deep enough to produce some heavy thunderstorms (see the radar-network display in Fig. 12(b)). (About an hour later, one of these storms became sufficiently intense to produce an F2 tornado.) The spacing of the shower lines is due to an intrinsic dynamical organization but further study of this dataset may indicate the extent to which the shape of the coastline, areas of modest hills, or other factors, may have assisted some of the shower lines to become more intense than others.

Figures 10 to 12 were given as examples of primary initiation. Next, in Figs. 13 to 17, we give examples of forcing in which a previous convective storm leads to the initiation of secondary convection.

The visible satellite image in Fig 13 shows an arc of convective cloud to the south-east of Chilbolton over the English Channel. At the time of Fig. 13, the Met Office network radar showed that a line of new convective showers was developing along this arc (not shown). The arc had formed along the gust front, or leading edge of a cold pool, due to the rain-chilled downdraft from an earlier mesoscale convective system that had formed on the western side of the CSIP area and drifted eastward. Data from the AWSs showed that a temperature drop of up to 8 C accompanied the passage of the gust front. Purdom (1982) showed that such visible satellite imagery is useful for identifying this important class of convergence line. The convergence at the gust front showed up as a velocity discontinuity on the Doppler radar PPI display - see the arc-shaped transition from green, through yellow, to red (in Fig.14(b)) at the leading edge of the main storm area in Fig.14(a).

Sometimes such a gust front shows up as a radar fine line as in Fig.15(a). The reflectivity pattern in this figure shows two clusters of convective showers, with a fine line 10 to 20 km ahead of them. The ZDR pattern in Fig. 15(b) shows the same shower systems (mainly green) at an earlier time, along with the outflow boundary to the east of one of them, characterized by a transition from red to green. Our working hypothesis is that the large values of ZDR in the red regions are due to insects in the unperturbed boundary layer whereas the low values of ZDR in the cold pool are from Bragg scattering in the relatively insect-free air of recent downdraft origin.

In another example of secondary initiation, a series of parallel lines of convective showers and thunderstorms developed (Fig. 16); the lines were transverse to the overall wind direction. Detailed observational and theoretical analyses (Morcrette et al. 2006; Marsham and Parker, 2006) indicated that these lines of

showers were triggered by gravity waves emanating from an earlier storm forming upwind of the CSIP area. Radar scans showing the top of the boundary layer were made with the 1275 MHz Chilbolton radar at a number of azimuths before and during the development of these storms. These scans were analysed so as to map the depth of the boundary layer out to a radius of about 30 km from Chilbolton (Fig. 17). A time series of plots like Fig. 17 indicated that the top of the boundary layer was modulated by a traveling gravity wave with wavelength 40 to 50 km and amplitude of the vertical air-parcel displacement of ± 150 m. The vertical sounding for this occasion was shown earlier in Fig. 2(a) and the accompanying Fig. 2(b) showed that a gravity wave capable of lifting the lid capping the boundary layer by a mere 150 m would indeed have been sufficient to enable convection to break through.

Examples of forcing from upper levels

The passage of upper-tropospheric PV maxima is the principal forcing mechanism from upper levels. A study by Roberts (2000) has shown that mesoscale PV maxima are abundant and are associated with a large proportion of the thunderstorms encountered in the north-east Atlantic area and in the more maritime parts of north-west Europe. The PV maxima are important for convection because of the associated patterns of advection and vertical motion. Advection of cold air into the upper and middle troposphere increases the CAPE and the ascent weakens the lid, i.e. reduces CIN. Because the cold air is also very dry it is often easily detected in satellite water vapor imagery and gives rise to the familiar water vapor (WV) dark zone (Browning, 1997). The analysis of WV imagery formed the basis of Roberts' analysis. An example from CSIP is given in Fig. 18 which shows a WV dark zone centred over central England. In the middle of the dark zone (due north of the Isle of Wight and

east of south Wales) is a very small gray dot which corresponds to an isolated thunderstorm. This storm occurred on the occasion depicted in Figs. 10 and 11. Detailed analysis shows it to have been due to the combined effects of the upper-level PV maximum and the coastally induced low-level convergence line discussed earlier which on its own produced only shallow convective showers.

The final example of an upper-level influence on convective initiation is shown in Fig. 19. Figure 19(a) shows a Eumetsat cloud-height product diagnosed from MSG satellite infrared channels. Figure 19(b) shows the corresponding visible image and Fig. 19(c) shows the radar network display for the same time. Orphaned anvils from decayed thunderstorms that had traveled northward from France are shown orange in Fig. 19(a); they appear as fuzzy light gray veils in Fig. 19(b). The shadowing from these anvils is thought to have slowed down the diurnal heating of the boundary layer very slightly, but just enough to account for the first deep convective cells being initiated outside or on the boundaries of the shadowed areas. The deep convective cells show up as bright clouds on the visible image (Fig. 19(b)). A few of these clouds were already developing into showers at this time (Fig. 19(c)) and some of them developed into thunderstorms that produced flash floods.

6 Using CSIP results to develop a high-resolution NWP model

The 4-km model discussed above is an intermediate step toward a nowcasting NWP system under development within JCMM which aims to produce very-short-range forecasts (0-6 h) using an NWP system based on a version of the Unified Model with horizontal resolution around 1 km. The performance of such a system can loosely be considered to depend on performance at three separate scales.

At the coarsest scale, the synoptic and mesoscale events determine the overall region where convection may occur. In practice, such regions are represented well by the current generation of operational NWP system. However, analysis errors are still present for important features such as small (~50 km) upper-level PV anomalies or low-level areas of enhanced moisture due to inadequacy of observations or the methods used to assimilate them.

Within this general region, there may be areas where instability triggers preferentially. As discussed above, these areas may be convergence lines due to surface forcing (e.g. sea-breezes) or due to previous storm outflows, or more two-dimensional regions due to other mechanisms. It is important to understand the mechanisms responsible for these areas so that the NWP model system can be designed to represent them accurately. For example, the representation of stable ‘lids’ is likely to depend on vertical resolution, while the representation of surface-forced convergence lines may depend on surface orography, sea- and land-surface temperatures and hence surface exchange processes. On the other hand, the development of convergence lines from storm downdrafts depends on the treatment of cloud dynamics and microphysics, as well as boundary-layer processes. The CSIP data are being used to validate and optimise the model formulation as well as to investigate the predictability of storms in the presence of different initiation mechanisms. This is important as many of these mechanisms operate before significant precipitation is observed by operational radar systems, and knowledge of them can help in the design of observing and assimilation systems.

On the smallest scale - within, for example, mesoscale convergence lines - individual storm cells develop. It is extremely unlikely that the location of such cells is generally predictable even within a very-high-resolution model. In a model with ~1-km resolution, cells develop from features (such as small cumulus clouds) that are not represented in the model. In practice, we find that the model behavior in generating individual cells depends critically on the representation of turbulence and its interaction with model dynamics, and that existing techniques require improvement. Two (related) approaches are conceivable. First, the transition from unresolved turbulence to explicit cells may be treated via ‘stochastic backscatter’, i.e. adding a well defined random component to physical parameterizations in the model. Second, understanding of these upscale transport mechanisms may enable new observing techniques (such as clear-air radar) to be used to detect regions that may develop into cells and thus modify the model state with sufficient lead-time to produce useful forecasts of subsequent precipitation. The CSIP data are providing a valuable source of validation data to improve our representation of these parameterization and assimilation issues.

Figure 20 shows an example of modelling progress so far for one of the cases discussed above (see Figs. 13 and 14). The figure shows a representation of broadband IR radiance temperature and surface rainfall rate from a 1.5-km, 76-level, model compared with MSG satellite IR radiance temperature and analysed radar rainfall using the NIMROD system. Figure 20(a) is a T+6.5 forecast, and it is notable that the organised area of showers over southern England is quite well forecast, if a little too far to the east. The role of the west coast is also clear in the forecast from the cloud streets that originate at or near the coast. Although their presence in observations is not obvious from the IR image in Fig. 20(b), which struggles to

resolve them, the visible MSG image in Fig. 13 hints at them and an even higher-resolution visible MODIS image (not shown) depicts them very clearly.

The Convective Storm Initiation Project (CSIP) was an international field campaign designed to observe the processes responsible for the initiation of convection in the UK. It was highly successful and provided unparalleled observations with which to understand and quantify these processes. Real progress is being and will continue to be made on improving forecasts of convective storms as a result of CSIP.

Acknowledgments

We are grateful to: Carolyn Cook, Alec Bennett, Nicky Chalmers, Helen Dacre, Laura Davies, Anna Fitch, Sarah Keeley, and Alexander Richardson, University of Reading; Markus Engelhardt, Roger Huckle, and Katrin Zink, Universität Karlsruhe; and Duncan Hodges and Mark Vowles, University of Bath for launching so many radiosondes. Olaf Stiller, JCMM, helped in the forecast centre at the University of Reading. Charles Kilburn and Ag Stephens, BADC, provided near real-time data products for forecasting and planning, and BADC provided workspaces and storing all data.

Martin Hill designed the AWSs; Ralph Burton assisted in building them; James Groves assisted in deploying them; Matt Hobby and Volker assisted with various aspects of the design. Martin Gallagher and Peter Kelly assisted in operating the Cessna aircraft. Charles Wrench helped with critical aspects of organising the field campaigns and operating the UV Raman lidar. Andrew Barkwith, University of Salford assisted with the Doppler lidar during the field campaigns. John Goddard and

the staff at Chilbolton Observatory: Owain Davies, Jan Lass, Eric Threlfall, Dave King, and Mal Clarke hosted the field campaigns and provided exceptional service.

CSIP exploited new instruments available through the (UK) Universities' Facility for Atmospheric Measurement (UFAM), which is funded by the Natural Environment Research Council following an initial award from the HEFCE Joint Infrastructure Fund. Operational observational and forecast data were provided by the UK Met Office. Satellite images are from Eumetsat. The Chilbolton Observatory, around which the project was based, is owned by the Council for the Central Laboratory of the Research Councils.

References

Barthlott Ch, U. Corsmeier, C. Meißner, F. Braun and Ch. Kottmeier 2006 The influence of mesoscale circulation systems on triggering convective cells over complex terrain. *Atmos. Res.* Doi:10.1016/j.atmosres.2005.11.010

Bennett, L. J.; Browning, K. A.; Blyth, A. M.; Parker, D. J.; Clark P. A. 2006: A review of the initiation of precipitating convection in the United Kingdom. *Q. J. R. Meteorol. Soc.* **132**. 1001-1020.

Browning, K.A. 1997: The dry intrusion perspective of extra-tropical cyclone development. *Meteorol. Appl.*, **4**, 317-324

Cullen, M.J.P. 1993: The unified forecast/climate model. *Meteorol. Mag.*, **122**, 81-94

Davies, T.; Cullen, M.J.P.; Malcolm, A.J.; Mawson, M.H.; Staniforth, A.; White, A.A.; Wood, N., 2005: A new dynamical core for the Met Office's global and regional modelling of the atmosphere, *Q.J.R. Meteorol.Soc.*, **131**, 1759-1782

Doviak, R.J. and Zrnica, D.S. 1993: Doppler radar and weather observations, 2nd edition. Academic Press, 562pp

Fabry, F. 2006: The spatial variability of moisture in the boundary layer and its effect on convection initiation: project-long characterization. *Mon. Wea. Rev.*, **134**, 79-91

Fabry, F., Frush, C., Zawadzki, I., and Kilambi, A. 1997: Extracting near-surface index of refraction using radar phase measurements from ground targets, *J. Atmos.Oceanic. Tech.*, **14**, 978-987

Goddard, J.F.W., Eastment, J.D. and Thurai, M. 1994: The Chilbolton Advanced Meteorological Radar: a tool for multidisciplinary atmospheric research. *Electronics and Communications Engineering Journal*, **6**, 77 – 86

Golding, B.W, 1998: Nimrod: a system for generating automated very short range forecasts, *Meteorol. Appl.*, **5**, 1-16

Gregory, D. and Rowntree, P.R. 1990: A Mass Flux Convection Scheme with Representation of Cloud Ensemble Characteristics and Stability-Dependent Closure. *Mon. Wea. Rev.*, **118** 1483-1506

Hoskins, B.J., McIntyre, M.E. and Robertson, A.W. 1985: On the use and significance of isentropic potential vorticity maps. *Q.J.R. Meteorol. Soc.*, **111**, 877-946

Jones, C.D. and Macpherson, B., 1997: A Latent Heat Nudging scheme for the Assimilation of Precipitation Data into an operational Mesoscale Model *Met Apps*, **4**, 269-277

Lorenc, A. C., S. P. Ballard, R. S. Bell, N. B. Ingleby, P. L. F. Andrews, D. M. Barker, J. R. Bray, A. M. Clayton, T. Dalby, D. Li, T. J. Payne and F. W. Saunders, 2000: The Met. Office Global 3-Dimensional Variational Data Assimilation Scheme. *Quart. J. Roy. Met. Soc.*, **126**, 2991-3012.

Marshall, J.H. and Parker, D.J. 2006: Secondary initiation of multiple bands of cumulonimbus over southern Britain. Part II: Dynamics of secondary initiation, *Q.J.R. Meteorol. Soc.*, **132**, 1053-1072

Morcrette, C.J., Browning, K.A., Blyth, A.M., Bozier, K.E., Clark, P.A., Ladd, D., Norton, E.G. and Pavelin, E., 2006: Secondary initiation of multiple bands of cumulonimbus over southern Britain. Part I: An observational case study. *Q.J.R. Meteorol. Soc.*, **132**, 1021-1051.

Purdom, F.J.W. 1982: Subjective interpretation of geostationary satellite data for nowcasting. In *Nowcasting*, K.A. Browning, Ed., Academic Press, 149-166

Roberts, N.M. 2000: The relationships between water vapour imagery and thunderstorms. JCMM Internal Report, **110**, 40pp. Available from JCMM, Dept. of Meteorology, University of Reading

Schmetz, J., Pili, P., Tjemkes, S., Just, D., Kerkmann, J., Rota, S. and Ratier, A. 2002: An introduction to Meteosat Second Generation (MSG). *Bull.Am. Meteorol. Soc.*, **83**, 977-992

Weckwerth, T.M. 2000: The effect of small-scale moisture variability on thunderstorm initiation. *Mon.Wea. Rev.*, **128**, 4017-4030

Weckwerth, T.M., Parsons, D.B., Koch, S.E., Moore, J.A., LeMone, M.A., Demoz, B., B., Flamant, C., Geerts, B., Wang, J. and Feltz, W.F. 2004: An overview of the International H₂O Project (IHOP_2002) and some preliminary highlights. *Bull.Am.Meteorol.Soc.*, **85**, 253-277

Wilson,J.W. and Schreiber,W.E. 1986: Initiation of convective storms at radar-observed boundary-layer convergence lines. *Mon. Wea. Rev.*,**114**, 2516-2536

Wilson, J. W. and R. D. Roberts, 2006: Summary of Convective Storm Initiation and Evolution during IHOP: Observational and Modeling Perspective. *Mon. Wea. Rev.*, **134**, 23-47.

Figure Captions

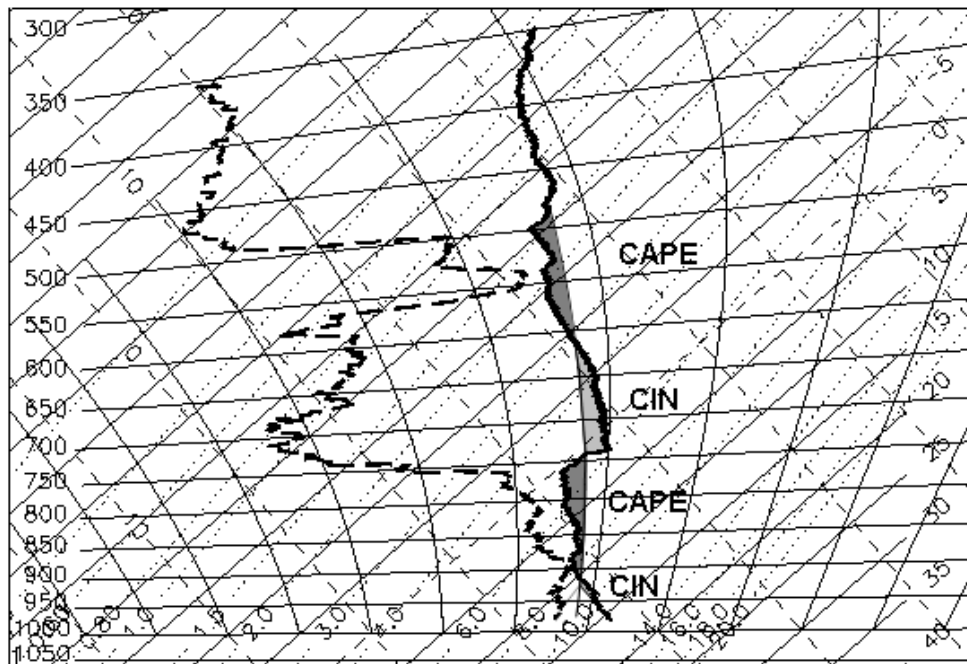


Figure 1: Tephigram for radiosonde launched from Bath at 1100 UTC on 15 June 2005 (IOP 1). The CAPE and CIN are shaded dark and light gray, respectively; the thin solid line partially bounding these areas is the 14C saturated adiabat representing a parcel that ascends unmixed from the boundary layer.

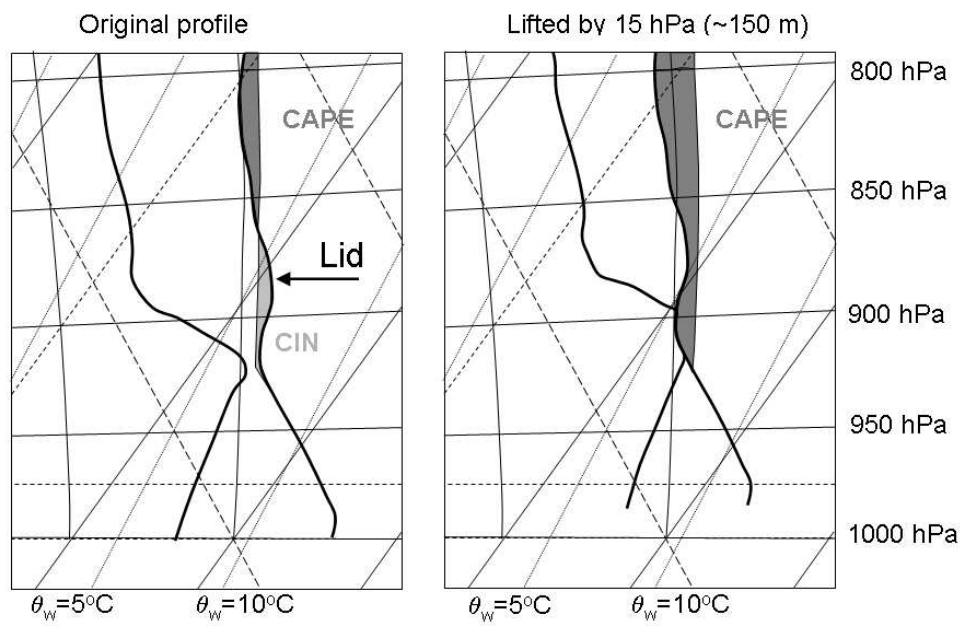


Figure 2: Illustration of how adiabatic lifting of a profile by as little as 15 hPa (about 150 m), can increase the CAPE and completely eliminate the CIN. The original profile is shown on the left and the lifted profile on the right. (Adapted from Morcrette et al. 2006).

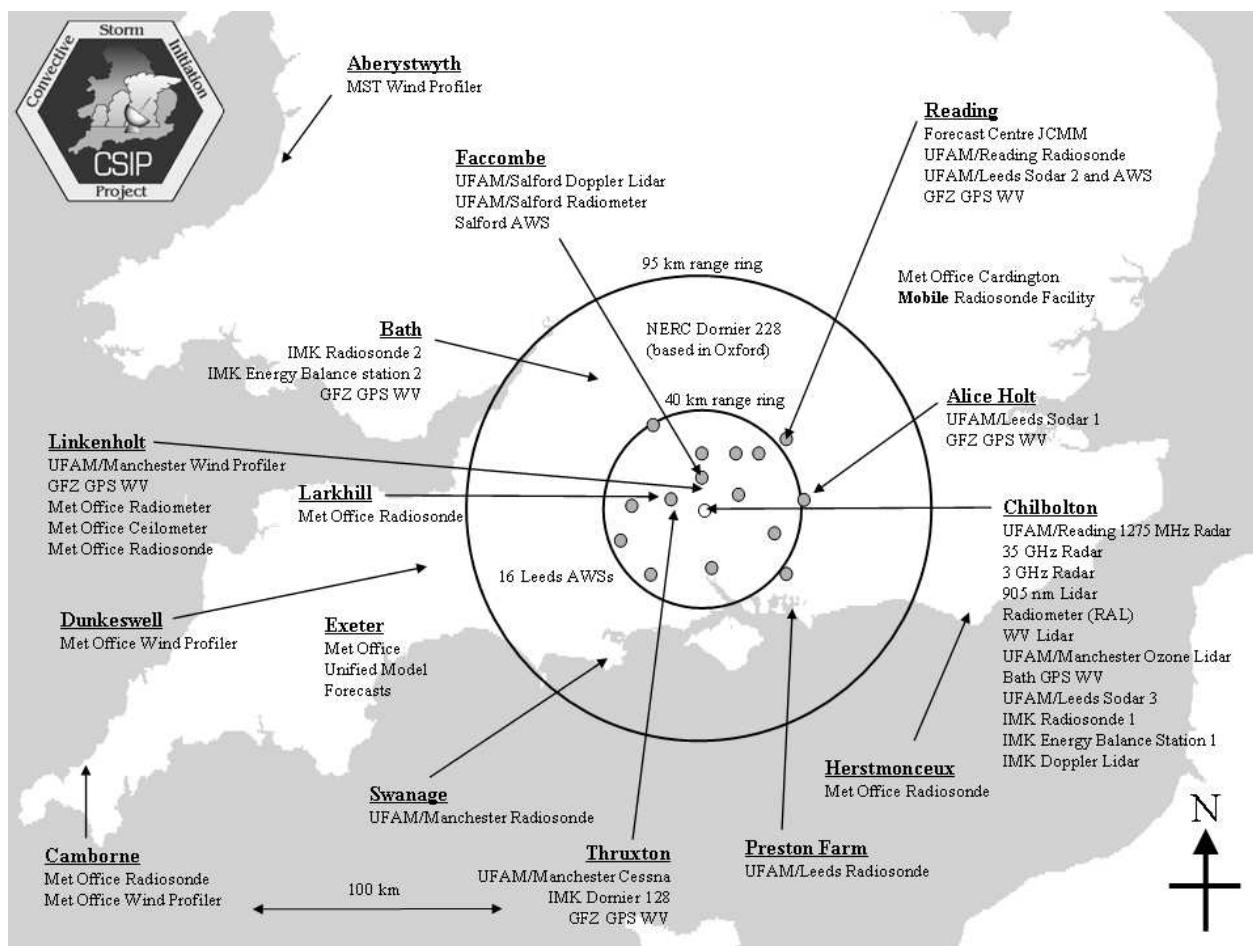


Figure 3: Map showing locations of instruments deployed in southern Britain during CSIP in June, July and August 2005. The shaded circles represent the position of the Automatic Weather Stations (AWSs).

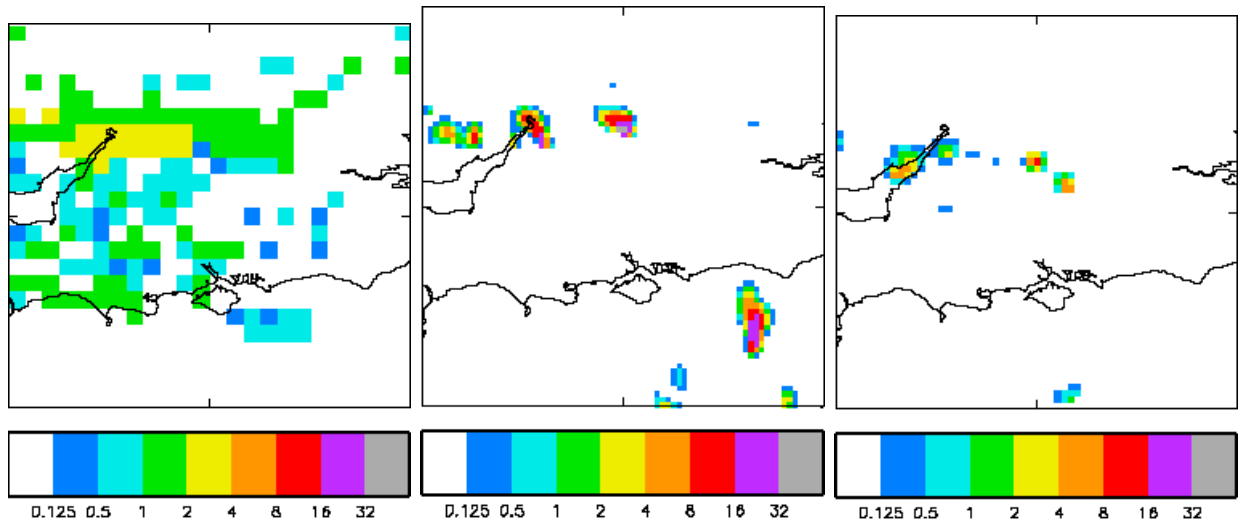


Figure 4: Example of a 13-h precipitation forecast from the Met Office Unified Model run using (from left to right) (a) a 12-km grid and (b) a 4-km grid, compared with (c) the rainfall rate observed by the weather radar network at 1300 UTC on 29 June 2005 (IOP 5). Key gives rainfall intensity in mm h^{-1} .

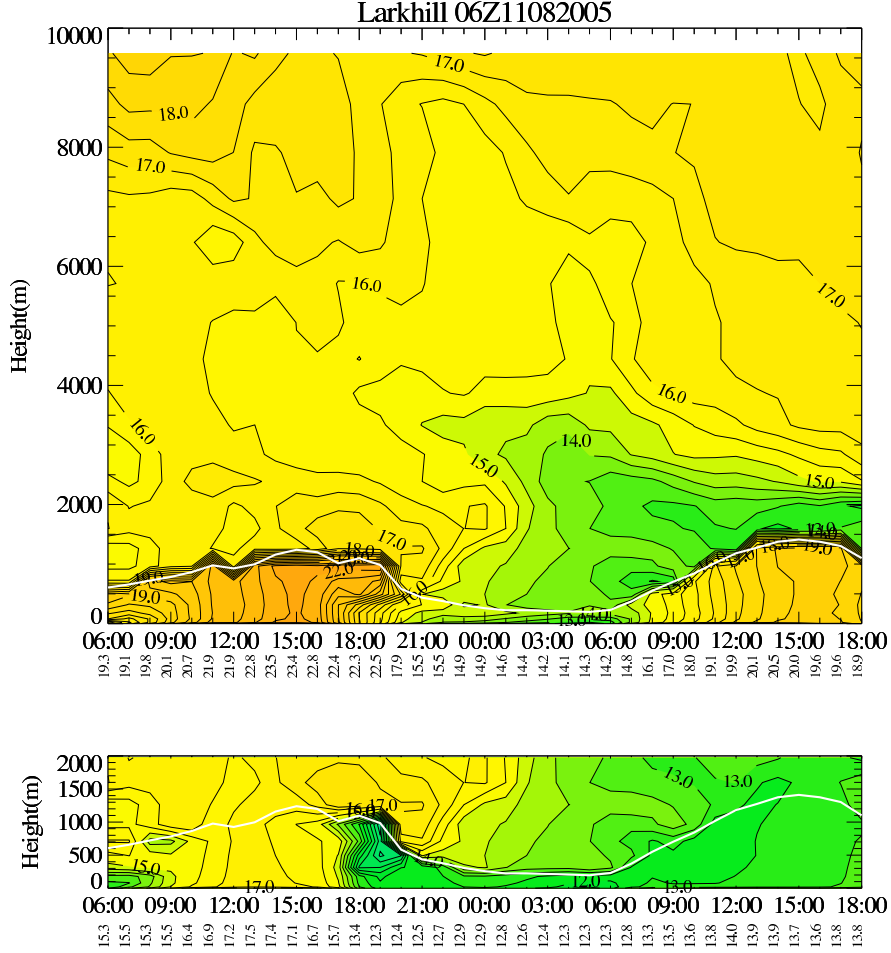


Figure 5: Met Office 12-km-grid Unified Model forecast of the time-height cross-section of θ_s over Larkhill (see Fig. 3 for location) on 11 August (IOP 14R) and 12 August 2005. The white line in the upper plot shows the lifting condensation level; above this the contours and shading represent θ_s and below they represent θ . (Surface values of θ are specified along the time axis of the upper plot). The lower plot shows θ_w .

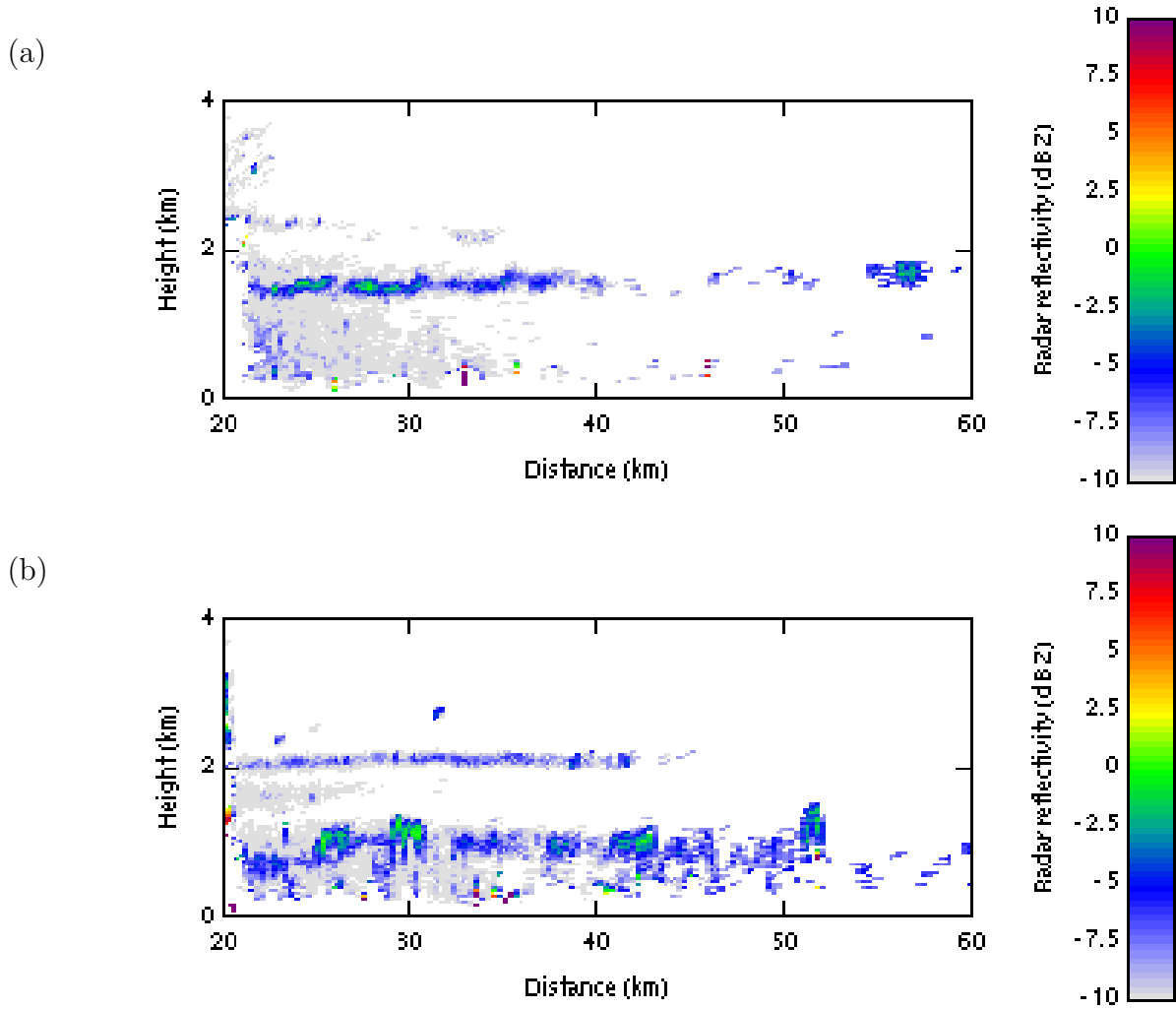


Figure 6: Two examples of RHI scans of reflectivity (dBZ) from the 3 GHz radar at Chilbolton showing lids and the outline of thermals: (a) echo from the bottom of a lid without significant convection beneath it; (b) thermals in the boundary layer below the bottom of a lid (at 1125 UTC on 18 July 2005 (IOP 9) and 1011 UTC on 29 June 2005 (IOP 5), respectively).

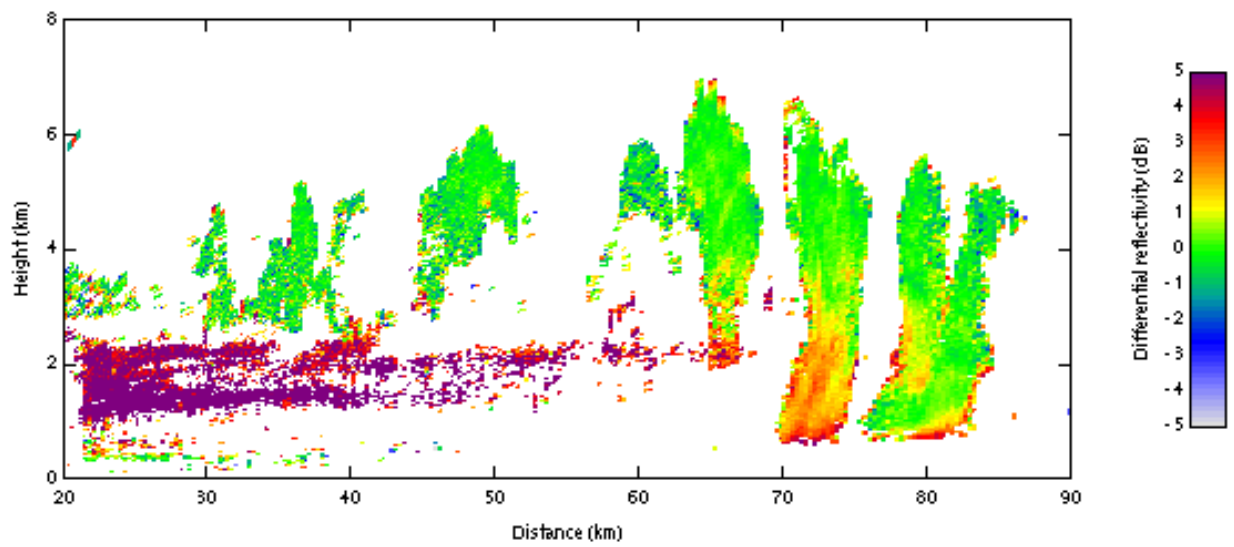


Figure 7: RHI of differential reflectivity (ZDR), from the 3 GHz Chilbolton radar, at 1249 UTC on 24 June 2005 (IOP 3), showing elevated convective cells forming above a stable frontal zone.

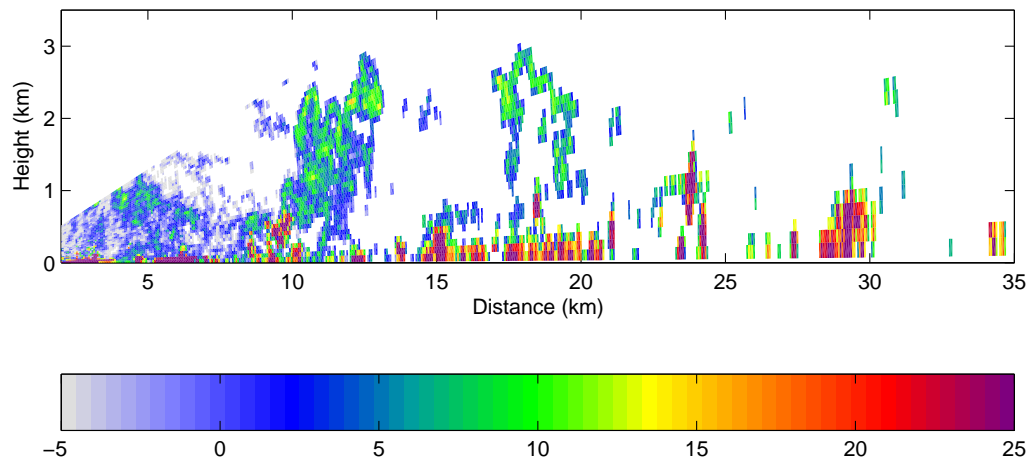


Figure 8: RHI of reflectivity (dBZ) from the 1275 MHz Chilbolton radar at 0928 UTC on 10 July 2004, showing developing cumulus congestus clouds. The echoes near the ground are a combination of ground clutter and returns from insects. (From Morcrette et al. 2006).

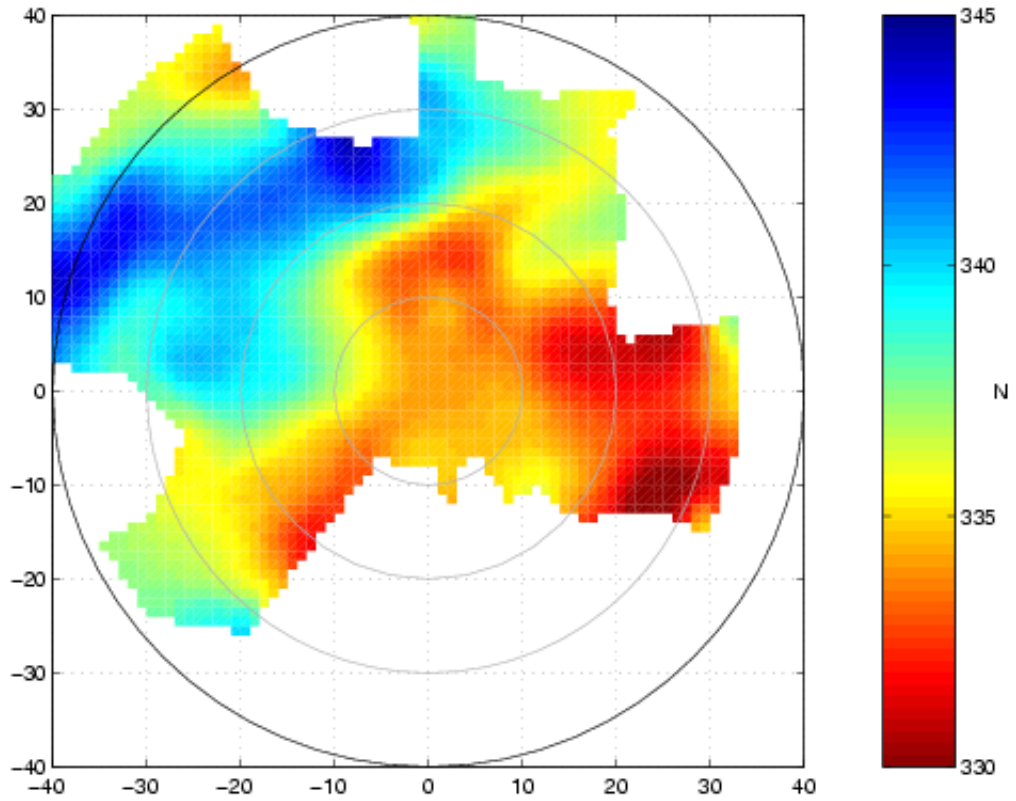


Figure 9: Refractivity field obtained from the 1275 MHz Chilbolton radar at 1259 UTC on 13 July 2005 (IOP 8), using the technique described by Fabry et al. (1997). In summer, the changes in refractivity are mainly due to humidity variations. Here, a change in refractivity of 1 N is approximately equal to a change in relative humidity of 1%.

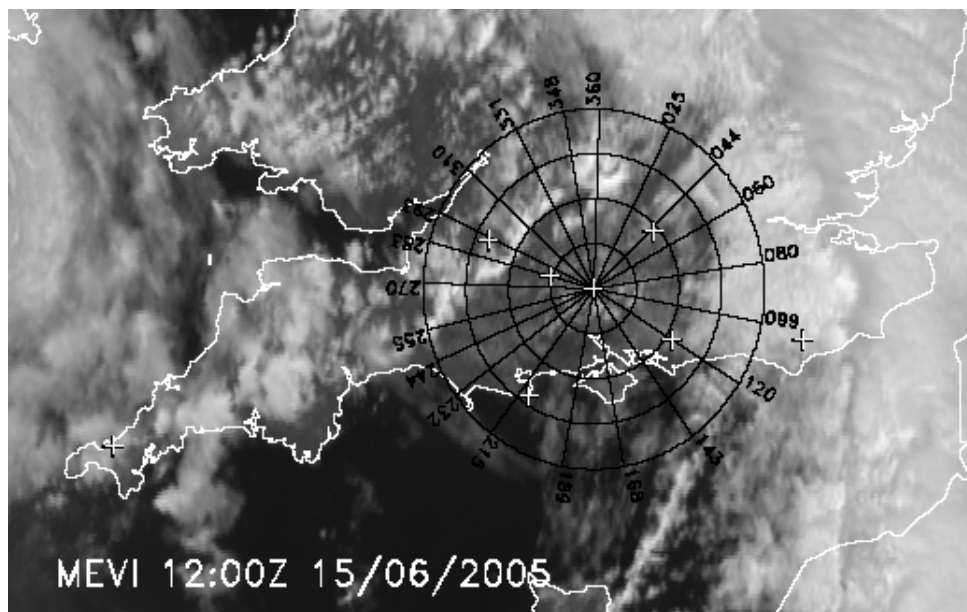
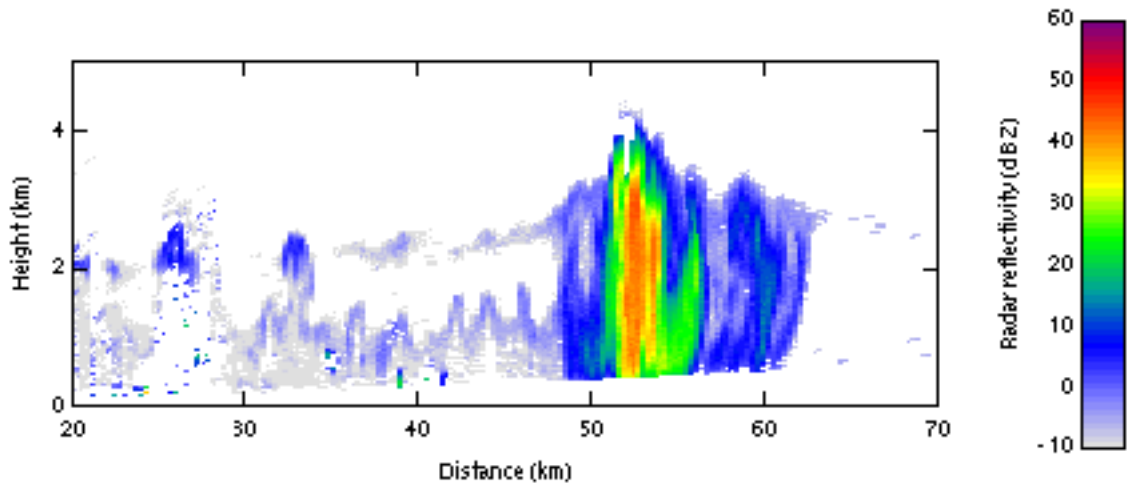


Figure 10: High-resolution visible image from Meteosat-8 (MSG) at 1200 UTC on 15 June 2005 (IOP 1), showing convective cloud along a convergence line extending from the south coast toward the north-east. Range rings are centered on Chilbolton and plotted every 25 km. The radial lines correspond to azimuths with low horizons along which series of RHI scans were obtained.

(a)



(b)

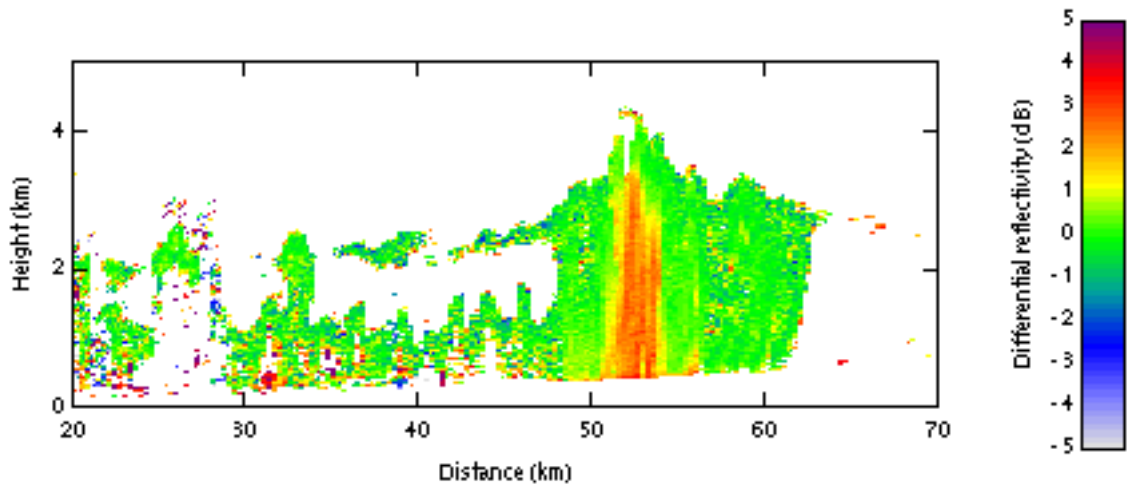


Figure 11: RHIs of (a) reflectivity (dBZ) and (b) differential reflectivity (dB) for a scan across the convergence line shown in Fig. 10, obtained from the 3 GHz Chilbolton radar at 1200 UTC on 15 June 2005 (IOP 1).

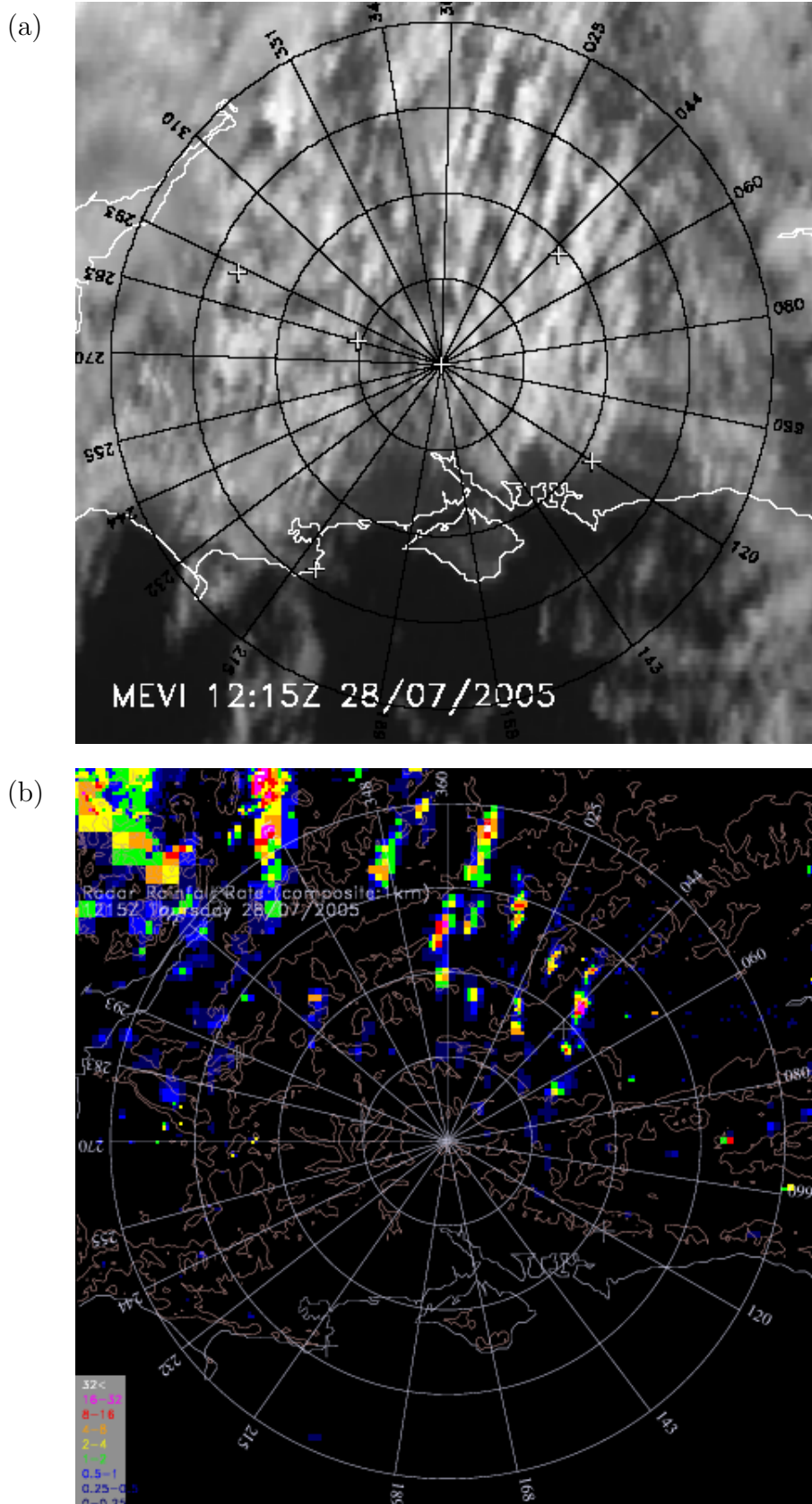


Figure 12: (a) High-resolution visible image from Meteosat-8 (MSG) and (b) rainfall rate from the radar network (key in mm h^{-1}) at 1215 UTC on 28 July 2005 (IOP 12), showing convective cloud streets and associated thunderstorms. Range rings are centered on Chilbolton and plotted every 25 km.

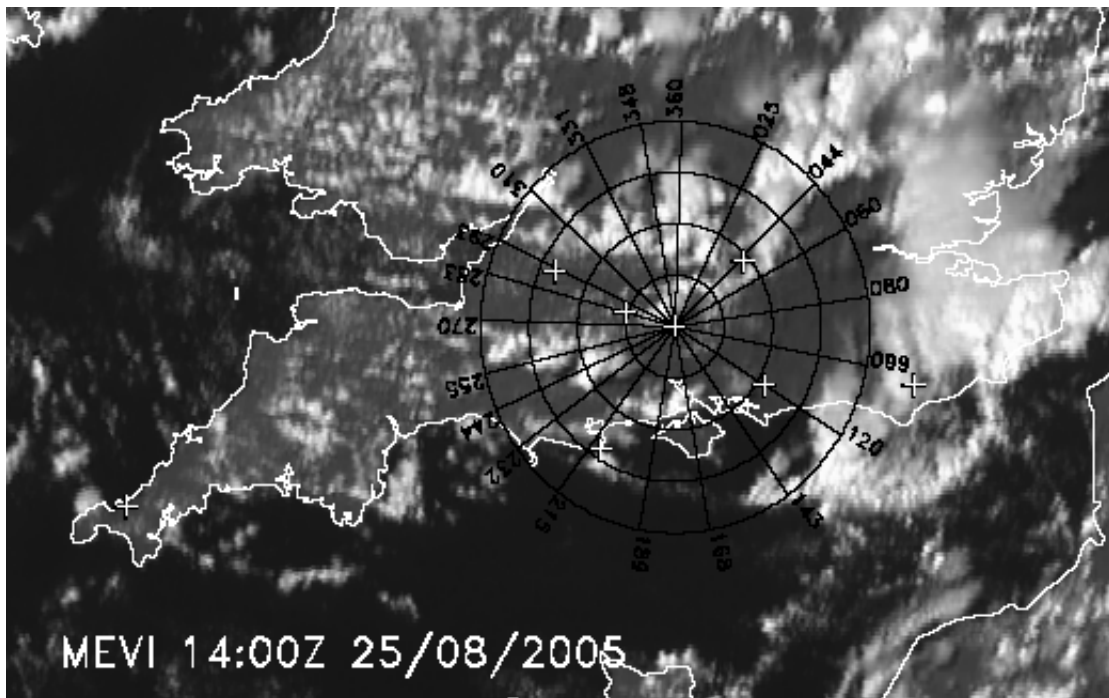
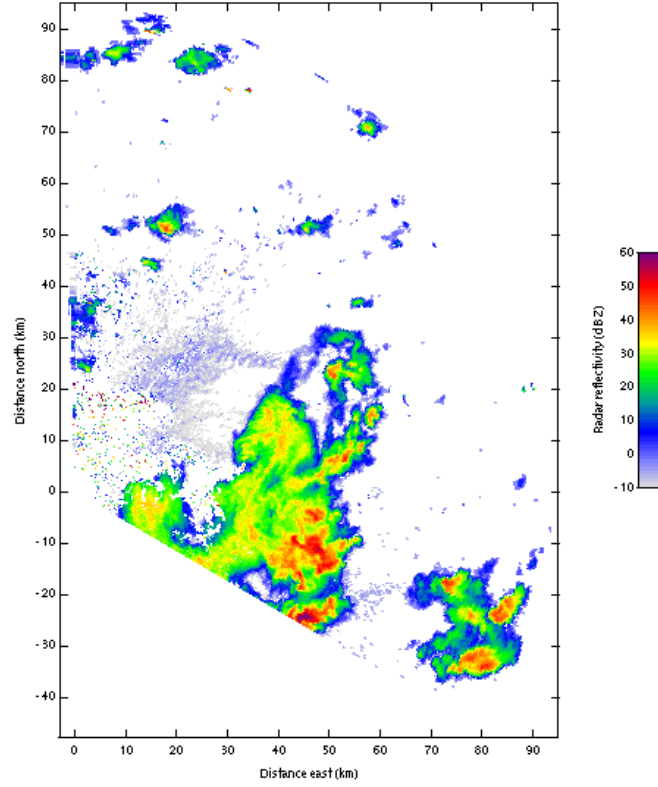


Figure 13: Similar to Fig. 10, but for 1400 UTC on 25 August 2005 (IOP 18), showing an arc of convective cloud along a gust front to the SE of Chilbolton over the English Channel.

(a)



(b)

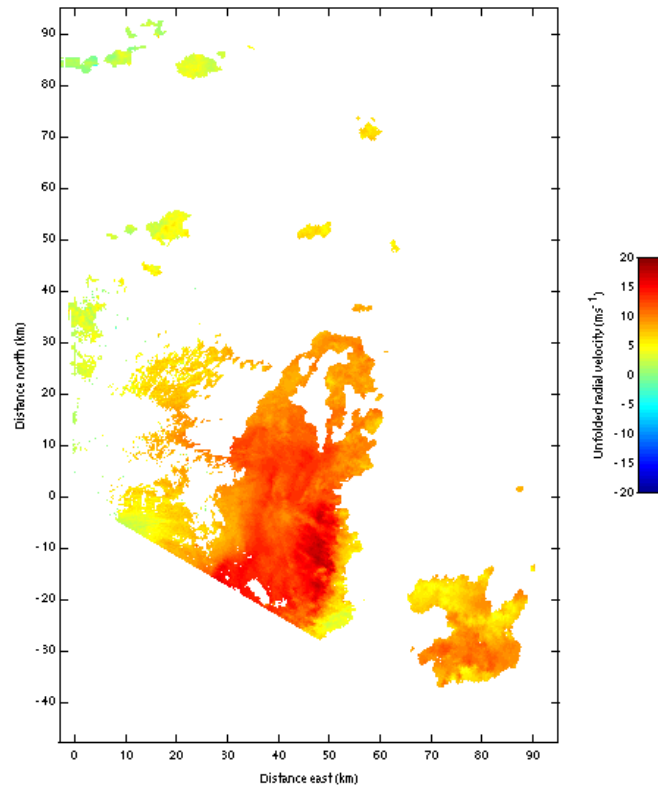
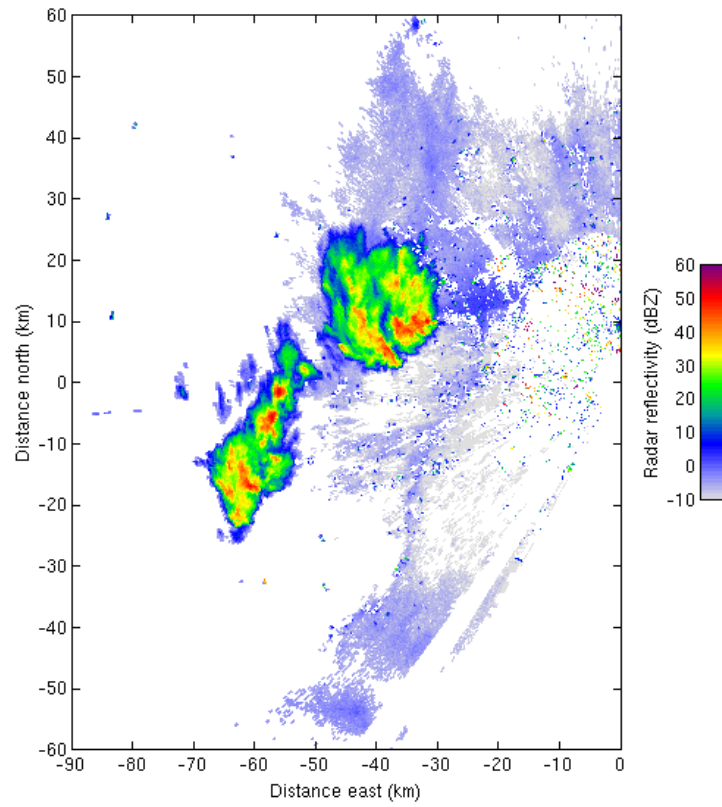


Figure 14: Example of a cold-pool-outflow convergence line: PPIs at 0.5 deg of (a) reflectivity (dBZ) and (b) unfolded Doppler velocity (m s^{-1} away from radar) at 1157 UTC on 25 August 2005 (IOP 18) showing the relation between convergence features and the precipitation field.

(a)



(b)

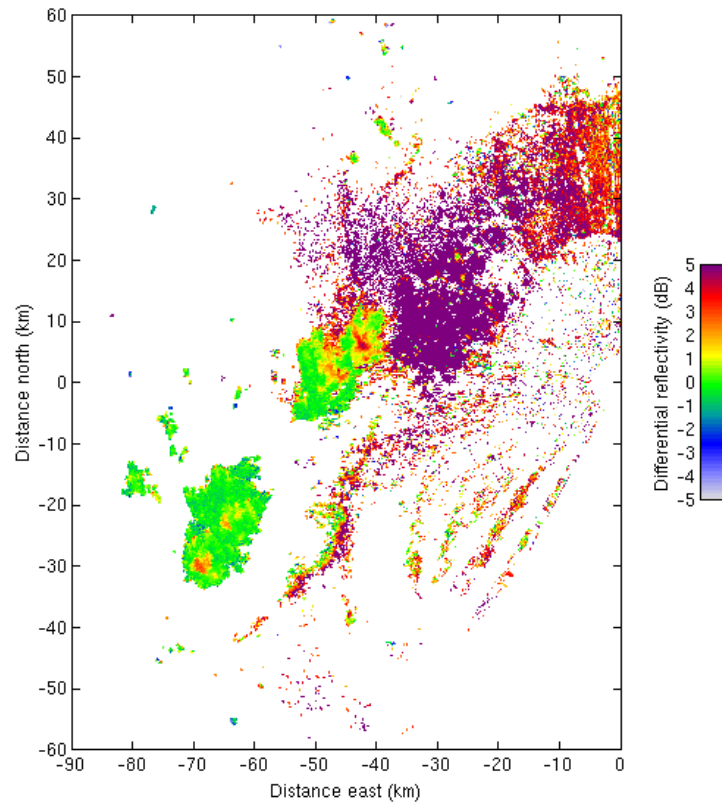


Figure 15: PPIs at 0.5 deg of (a) reflectivity (dBZ) at 1701 UTC and (b) differential reflectivity (dB) at 1622 UTC on 18 August 2005 (IOP 16), showing a radar fine line associated with a gust front.

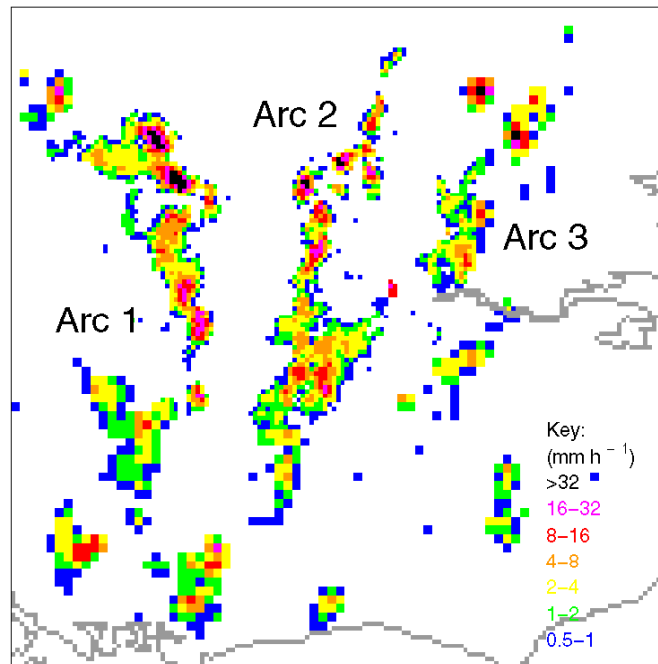


Figure 16: Rainfall rate (mm h^{-1}) over a $150 \text{ km} \times 150 \text{ km}$ region of southern England at 1130 UTC on 10 July 2004, showing a series of precipitation bands that had been triggered by a gravity wave generated by an earlier storm. (From Morcrette et al. 2006).

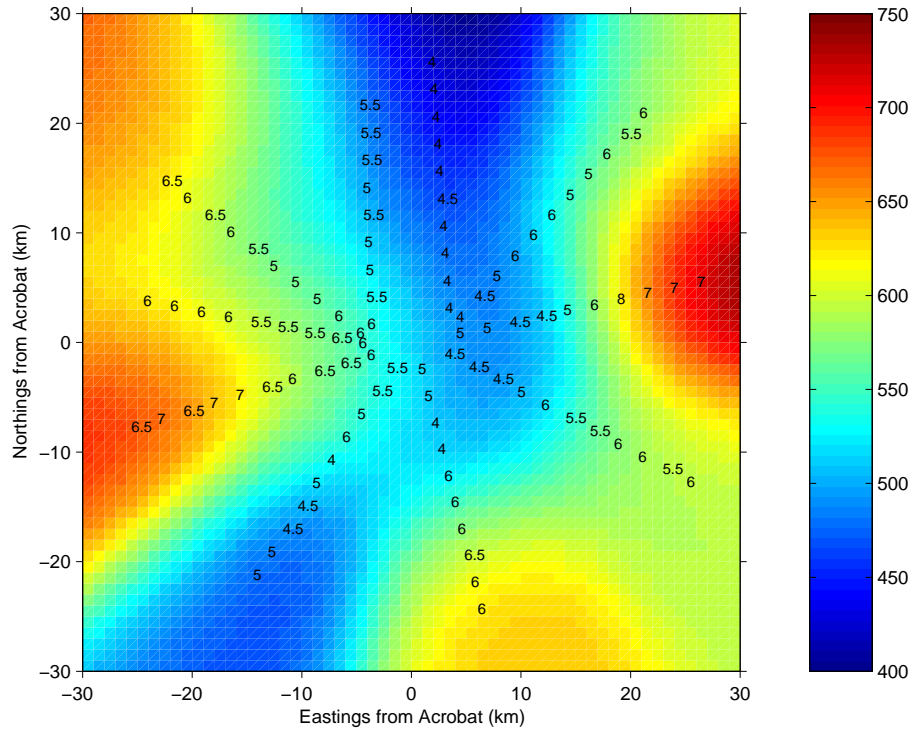


Figure 17: Height of boundary-layer top (hundreds of meters), with interpolated heights shown in color (according to the key, in meters) as derived from ten RHI scans with the 1275 MHz Chilbolton radar. The variation in height is believed to be due to the gravity wave that triggered the precipitation bands in Fig. 16. The scans were obtained from 0751 to 0807 UTC and their positions have been displaced to correspond to 0758 UTC assuming a system velocity of 8 m s^{-1} from the west. (From Morcrette et al. 2006).

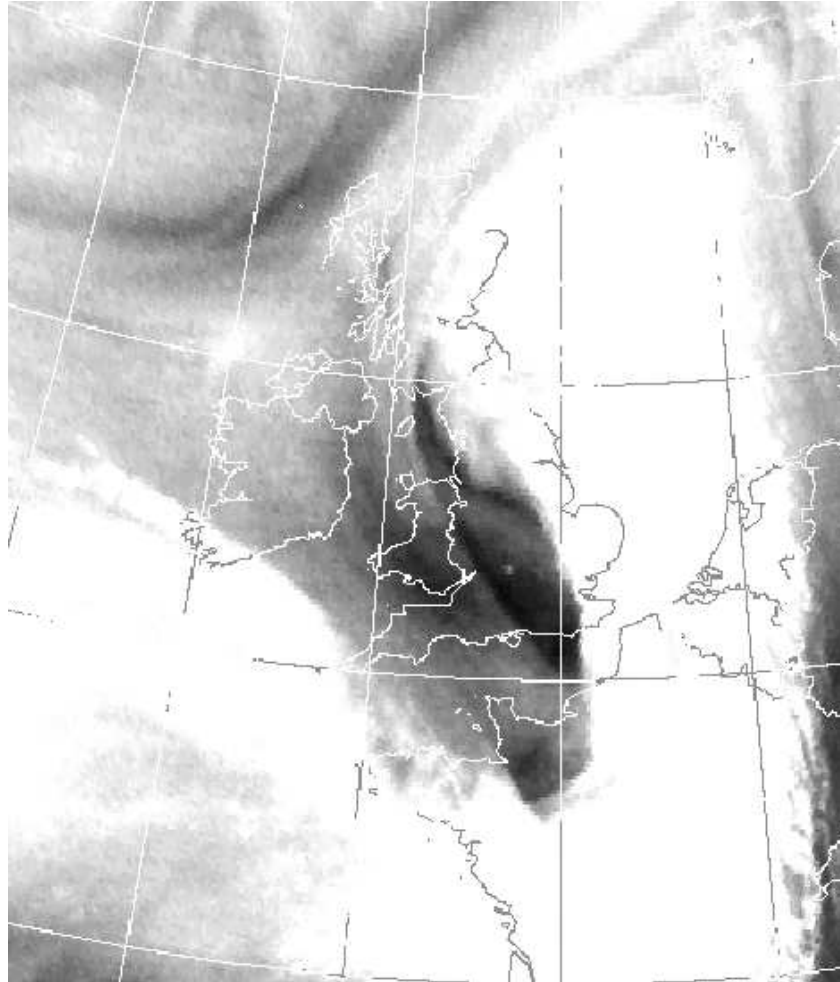


Figure 18: Rapid-scan Meteosat water-vapor image at 1200 UTC on 15 June 2005 (IOP 1), showing a thunderstorm (very small gray dot) within a water vapor dark zone. The image is enhanced to clarify the position of this thunderstorm with respect to the dark zone; although the surrounding white areas are saturated, there is no information in these areas relevant to the discussion. Because the thunderstorm was shallow, it does not show up as a major feature in the water vapor imagery which is sensitive mainly to features in the upper troposphere.

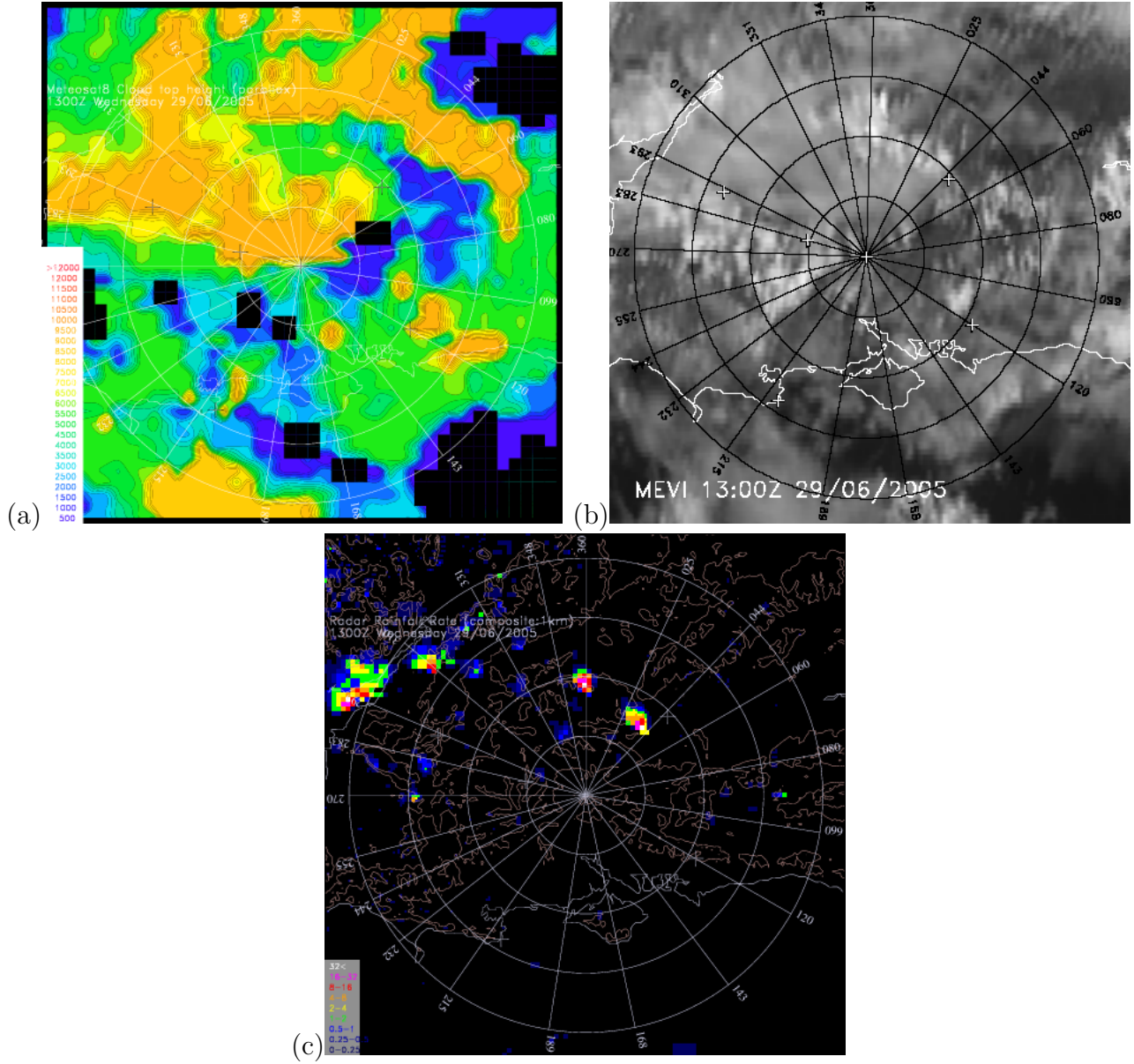
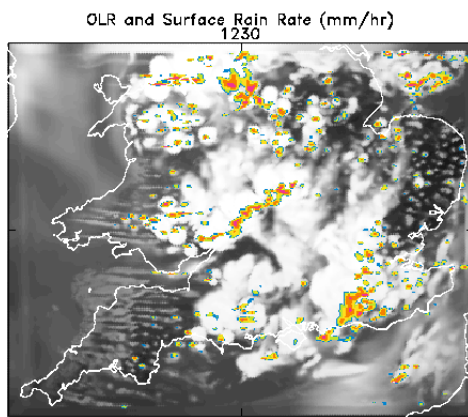


Figure 19: (a) Cloud-top height (m) derived from MSG infra-red data, (b) MSG high-resolution visible image and (c) radar-network rainfall rate, at 1300 UTC on 29 June 2005 (IOP 5), showing the possible effect of shadowing by cirrus anvils on the formation of new convective clouds. Range rings are centered on Chilbolton and plotted every 25 km.

(a)



(b)

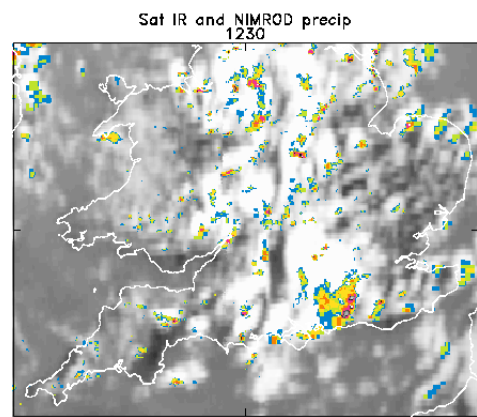


Figure 20: (a) Unified Model 6.5-hour forecast of broadband IR radiance temperature and surface rainfall rate compared with (b) observational analysis showing NIMROD-derived rainfall rate (colors) superimposed on IR satellite-derived cloud (white), at 1230 UTC on 25 August 2005 (IOP 18).